THE ASTROPHYSICAL JOURNAL, 165:285–294, 1971 April 15

MASS LOSS FROM M STARS

R. D. GEHRZ* AND N. J. WOOLF*
University of Minnesota, Minneapolis
Received 1970 September 14; revised 1970 November 21

ABSTRACT

Infrared observations of M giants and supergiants show that circumstellar dust shells are frequently present. The observations permit the radii and densities of the dust shells to be determined. It is shown that radiation pressure drives the particles through the gas at a velocity that varies with the density The momentum coupling drives the gas out of the star. Velocities of gas ejection are estimated and compared with optical and radio measures. Rates of mass ejection are calculated for a number of stars. These rates are compared with the rates required to maintain the interstellar medium at its present density.

I. INTRODUCTION

The rate of mass loss from late-type stars is very poorly known. Yet it affects processes of stellar evolution and the chemical composition of interstellar matter, and it may have a bearing on the questions of distribution and nature of large solid bodies in the Universe.

Optical methods of determining the rate of mass loss from cool stars have been attempted by Weymann (1962). These methods are limited to a very few bright stars. Further, although the outflow velocity is well determined, the density in the shell and the size of the region where the flow commences are poorly determined, so the rate is left uncertain.

A new approach has become possible as a result of the detection of circumstellar silicate emission around M stars (Woolf and Ney 1969; Gilman 1969). This matter apparently becomes a major part of the interstellar dust. It is visible in emission (Ney and Allen 1969; Stein and Gillett 1969) and in absorption (Hackwell, Gehrz, and Woolf 1970), and appears to form about 0.4 percent of the interstellar medium by mass.

Observations of circumstellar emission give new information about the density and dimensions of the dust envelopes. Observations of some stars, presented here, show the silicate envelopes to be optically thick near the peak. In such cases the "line profile" of the emission can give evidence both of the optical depth of the dust and of its amount. Thus the density and dimensions of the dust shells can be found. The density of the dust shells can be related to the gas density if complete condensation of silicon is assumed. However, by continuity, the density ratio changes if the dust velocity through the gas is comparable with or greater than the gas velocity from the star. In these cases, the present method determines a lower limit to the rate of mass flow from the star. Some simple corrections for this factor are attempted. Fortunately, in certain critical cases, such as in the rate of mass loss from Mira variables, it will appear that these corrections are not important. For some supergiants, however, they become appreciable.

II. THE MECHANISM OF MASS LOSS

In a study of polarization, Dyck *et al.* (1971) argued that circumstellar dust shells are relatively thin structures well separated from the stars. Further evidence from the infrared observations discussed in § IV supports this model. There are two simultaneous conditions to be fulfilled for matter to condense. The radiation density which would determine the particle temperature must be low. The gas density, which sets a

* Visiting astronomers, Kitt Peak National Observatory, which is operated by the Association of Universities for Research in Astronomy, Inc., under contract with the National Science Foundation

lower limit on the particle vapor pressure, must be high. The first condition does not seem to be satisfied inside the photospheres of stars. However, both conditions could be fulfilled if cool stars were surrounded by extensive atmospheres.

The observations of eclipsing binaries such as ζ Aur and VV Cep (Wilson 1960) show the presence of gas at large distances from the photospheres of late-type stars. The observation of circumstellar dust in emission is taken as further evidence that the scale heights of the atmospheres are comparable with the size of the stars.

When the dust condenses, radiation pressure rapidly accelerates it through the gas, and it acquires a terminal velocity. The further momentum imparted to the dust accelerates the gas. The visual observations show the flow to be supersonic. The detailed determination of the rate of mass flow must therefore occur in the thin zone where the grains are formed and accelerated. The infrared observations are presumed to refer mainly to the region just outside this where the dust density is high. Thus the infrared observations are more suitable for giving information on the rate of mass loss than on the mechanism operative in the subsonic region of the flow.

Late-type stars near the peak of the giant branch should have convective velocities at the surface which are comparable to sonic speeds (Stein 1966). Thus even though sonic and convective velocities are individually smaller than escape velocities, they will combine to give a large scale height. Possible magnetic support of the atmosphere may further help develop a large scale height, while the condensation of rare nonvolatile substances in the photosphere may provide further support in extending the scale height. Action of radiation pressure on molecules may also be important.

This discussion suggests that those late-type stars which develop extended atmospheres will be able to condense solids, and that this condition simultaneously generates dense outflowing envelopes. A similar mechanism operative for carbon stars has been discussed by Wickramasinghe, Donn, and Stecher (1966).

In some hotter pulsating stars, shock waves may eject matter (Gehrz and Woolf 1970), and radiation density and gas density in the ejected matter may be adequate for solids to condense; but the phenomenon is probably different from that in the cool stars, and is being further investigated. In hot stars there are often ionized gas shells in which ultraviolet radiation pressure and perhaps magnetic coupling cause the outflow. In these flows the radiation density may often fall low enough for solids to condense; however, the composition of condensates in these cases, planetary nebulae, Be stars, etc., may no longer be consistent with calculations of chemical equilibrium (Arrhenius and Alfvén 1971).

Under different circumstances all three of these mechanisms may be appropriate to late-type stars. In this paper, however, we shall concentrate our attention on M-type stars without bright hot companions and assume only the mechanism of radiation pressure acting on grains.

III. OBSERVATIONS

Initially, broad-band measures of stars at 3.5 and 11.5 μ were made from the O'Brien Observatory. Later, photometers with passbands at 8.5 and 5.0 μ were also used. At Kitt Peak a single photometer responding at 11.0, 8.4, 4.9, and 3.5 μ was developed by Gillett and Stein (1971).

The zero point of the magnitude systems was set to be on the UBV–Arizona system. Colors of three bright A stars were extrapolated to 11.5 μ by assuming that colors lay on a linear plot[1] against $1/\lambda$. Colors of bright standard A stars were used at other wavelengths by a process of interpolation.

Absolute calibration at 11.5 μ was separately derived by three methods. Observations by Ney (1969) of the planet Mercury near superior conjunction were used to provide a

[1] For frequencies below $\nu = kT/h$ the slope of such lines for blackbodies is predicted to be one half of that given by Hardie (1962) for spectral regions where the Wien approximation is valid.

calibration on the assumption that the surface of Mercury radiates like a blackbody. A second calibration came from an observation of the G dwarf η Cas A. The solar emission has been measured in the 10-μ region by Saiedy (1960), and η Cas A was assumed to follow the same spectral energy distribution in the infrared. Remarkably, these two calibration objects differed in flux by 10^5, and so provided some check on linearity of the equipment. Finally, the flux from Vega at 11.5 μ was predicted from the 3.5-μ flux by Johnson (1965) under the assumption that its spectral energy distribution followed a Rayleigh-Jeans distribution. The mean calibration appeared to have an uncertainty of 10 percent.

Recently Gillett and Stein (1971) have independently calibrated the photometer at Kitt Peak. Our 11.5-μ calibration translates by a Rayleigh-Jeans law to an 11.0-μ calibration: zero magnitude $= 33.5 \pm 3.4 \times 10^{-26}$ W m^{-2} Hz^{-1}. Gillett and Stein give 35.0, which is in satisfactory agreement. Further, the magnitude scale derived independently by Gillett and Stein seems to differ by less than typical observational errors from the scale we have derived.

The results of the observations of a variety of stars are given in Table 1. Not all of them are used here, but they are given for general usage. The table is divided into sections for main-sequence stars, nonvariable or mildly variable giants, M-type variable giants, carbon stars, supergiants, and binaries. Observations of yellow variable stars are given elsewhere (Gehrz and Woolf 1970), and Be stars are discussed by Woolf, Stein, and Strittmatter (1970). Further supergiants have been observed by Gehrz, Ney, and Strecker (1970). Gillett and Stein (1971) list B stars associated with nebulosity. Gillett, Merrill, and Stein (1971) present data on late-type stars that have independent observations with about 40 percent overlap of objects in our Table 1. Gillett, Hyland, and Stein (1970) list some intermediate-type supergiants. In the figures of this paper, data from Gillett, Merrill, and Stein have been used as well as the data in Table 1.

IV. COLOR-COLOR DIAGRAMS

Two useful colors can be derived from the observations. At 3.5 μ the optical depth of the silicate envelope is minimal for both its absorption and its emission effects. At 11 μ, silicates have their peak emissivity, but often become optically thick. At 8.4 μ, on the edge of the silicate peak, the emission has such a low optical depth that it rarely becomes saturated; however, the optical depth is sufficient to produce measurable effects. Then the color (3.5) − (8.4) measures silicate emission, and the color (8.4) − (11) can be used to measure optical depth. From the nonvariable giants in Table 1, it seems that the intrinsic colors of these stars are 0.0, 0.0. Thus stars for which the optical depth of the envelope tends to zero will be found at the origin.

Consider an emitting zone around a star in a thin spherical shell, assumed to have the same temperature as the star. The flux at a wavelength λ is:

$$F_\lambda = F^*_\lambda \left\{ \left[\left(\frac{R_{\text{shell}}}{R^*} \right)^2 - 1 \right] (1 - e^{-\tau_\lambda}) + 1 \right\} , \tag{1}$$

where F^* is the flux from the star alone and τ_λ is the average optical depth of the shell to its own emission. Consider the optical depth at three wavelengths to differ. Then as the optical depth of the envelope is increased, the colors will execute a curve in a color-color diagram.

In Figure 1 we assume that the shell radius is either 10 times or 4 times the stellar radius, and that the ratio of optical depths 11 μ:8.4 μ:3.5 μ is 8:1:0. Supergiant stars are shown in this plot, and a blackbody line is shown for comparison. If the shell is cooler than the star, the same curves are closely correct down to shell temperatures of $\sim$500° K; however, the shell size is increased relative to the star size by $(T^*/T_{\text{shell}})^{1/2}$.

Since the curves seem to explain the deviations from the blackbody line, we can infer

TABLE 1

STARS OBSERVED

Star	3.5 μ	4.9 μ	8.4 μ	11 μ	[3.5] −[11]	dM/dT $\times 10^{-6}$ $M_\odot$ yr^{-1}	Spectral Type	Variable Type
Supergiants								
1. δ CMa	+0.25	+0.09	−0.03	−0.06	0.31	...	F8 Ia	...
2. o^1 CMa	−0.04	+0.21	−0.00	−0.23	0.19	...	M0 Iab	...
3. μ Cep	−2.06	−2.06	−2.85	−4.17	2.11	10	M2 Ia	SRc
4. RW Cep	+1.55	+1.38	+0.46	−1.23	2.88	5	K5 Ia–0	Ic
5. α Cyg	+0.71	+0.77	+0.81	+0.83	−0.12	...	A2 Ia	...
6. RW Cyg	−0.06	−0.03	−1.00	−2.76	2.70	5	M2 Ia–ab	SRc
7. BC Cyg	−0.29	−0.25	−1.20	−3.12	2.83	7	M3.5 Ia	Ic
8. BI Cyg	−0.02	+0.04	−1.14	−2.85	2.83	7	M3 Iab	Ic
9. TV Gem	+0.59	+0.70	...	−1.30	1.89	1.2	M1 Iab	SRc
10. α Ori	−4.52	−4.16	−4.76	−5.56	1.04	0.7	M2 Iab	SRc
11. S Per	+0.35	−0.11	−1.20	−2.89	3.24	27	M4 Ia	SRc
12. UY Sct	+0.33	+0.11	−0.43	−2.39	2.72	6	M4 Ia–ab	?
13. AX Sgr	+2.41	+2.40	+1.87	−0.68	3.09	6	G8 Ia	SRc
14. 119 Tau	−1.21	...	...	−1.26	0.05	...	M2 Ib	SRc
15. HR 8752	+1.10	+0.93	+0.36	+0.43	0.67	...	G0 Ia	...
16. HD 168607	+3.15	+2.42	+2.56	+2.77	0.38	...	B9 I$^+$ap	...
17. HD 168625	+3.82	+3.01	+1.80	+1.14	2.68	...	B8 I$^+$e	...
18. HD 183143	+3.22	+3.11	+2.73	+2.95	0.27	...	B7 Ia	...
Dwarfs								
19. α Aql	...	...	...	+0.26	...	...	A 7	...
20. α CMa	−1.47	−1.39	−1.43	−1.59	0.12	...	A1 V	...
21. α CMi	−0.75	−0.64	−0.80	−0.86	−0.09	...	F5 IV	...
22. η Cas A	...	...	...	+1.94	...	...	G0 V	...
23. α Lyr	+0.01	−0.02	−0.05	−0.03	0.04	...	A0 V	...
24. α Vir	+1.62	+1.45	+1.70	+1.78	−0.16	...	B1 V	...
25. Lall 21185	+3.09	+3.38	+2.72	+2.32	0.77	...	M2 V	...
Nonvariable (or Mildly Variable) Giants								
26. α Aur	−1.97	−1.72	−2.00	−2.01	0.04	...	G5 III	...
27. β And	−2.05	−1.60	−2.00	−2.01	−0.04	...	M0 III	...
28. α Boo	−3.13	−3.00	−3.19	−3.27	0.14	...	K2 III	...
29. α Cet	−1.89	...	...	−1.97	0.08	...	M2 III	...
30. 40 Com	−0.37	−0.10	−0.43	−0.62	0.25	...	M5	...
31. γ Dra	−1.44	−1.18	−1.34	−1.52	0.08	...	K0 III	...
32. β Gem	−1.19	−1.14	−1.29	−1.33	0.14	...	K0 III	...
33. η Gem	−1.63	−1.09	...	−1.76	0.13	...	M3 III	SRb
34. μ Gem	−2.01	...	...	−2.14	0.05	...	M3 III	...
35. π Leo	+0.21	+0.78	+0.37	+0.27	0.06	...	M2 III	...
36. 72 Leo	−0.27	−0.02	−0.26	−0.38	0.11	...	M3 III	...
37. 75 Leo	+1.19	+1.41	+1.23	+1.01	0.18	...	M0 III	...
38. δ^2 Lyr	−1.45	−1.08	...	−1.66	0.21	...	M4 II	?
39. β Peg	−2.45	−2.05	−2.39	−2.49	0.04	...	M2 II–III	Ib
40. ρ Per	−2.14	...	...	−2.23	0.09	...	M4 II–III	SRb
41. σ Sco	+2.14	+1.97	+1.82	+1.66	0.48	...	B1 III	...
42. α Tau	−3.02	−2.66	−2.97	−2.99	−0.03	...	K5 III	...
43. μ UMa	−0.95	−0.64	−0.87	−1.11	0.16	...	M0 III	...
44. δ Vir	−1.38	−1.26	−1.39	−1.63	0.25	...	M3 III	...
45. ω Vir	−0.33	+0.04	−0.24	−0.57	0.24	...	M6	...
46. +20°257	+1.44	+1.62	+1.54	+1.10	0.34	0.06	M4	...
47. +30°220	+1.22	+1.35	+0.80	−0.17	1.39	0.8	M8	...
M Giant Variables								
48. R Aql	−1.19	−1.24	−1.76	−2.87	1.68	0.8	M5–M8	M
49. R Boo	+1.18	...	...	+0.42	0.76	0.1	M3–M6	M
50. W Boo	+0.13	+0.30	−0.02	−0.22	0.35	0.05	M3 III	?
51. RV Boo	−0.33	−0.27	−0.58	−1.56	1.23	0.28	M5–M7	SRb
52. RW Boo	+0.26	+0.37	−0.14	−0.96	1.22	0.28	M5	SRb
53. RX Boo	−2.25	−1.95	−2.80	−3.61	1.36	0.4	M7–M8	SRb
54. R Cas	−2.06	−2.18	...	−4.08	2.02	1.2	M6–M8	M
55. T Cas	−1.52	...	...	−2.61	1.09	0.4	M6–M8	M
56. R Cnc	−1.33	−0.88	−1.49	−2.55	1.22	0.6	M6–M8	M
57. RS Cnc	−2.07	−1.61	−2.26	−2.95	0.88	0.4	M6 Ib–II	SRc?
58. R CVn	−0.05	−0.09	...	−1.39	1.34	0.5	M6–M8	M
59. V CVn	+0.78	+0.64	−0.31	−1.53	2.31	1.2	M4–M6	SRa
60. S CrB	−0.60	−0.98	−1.98	−2.83	2.23	4	M6–M8	M
61. χ Cyg	−2.25	−2.57	−3.21	−4.00	1.75	2.8	S7,1–S10,1	M
62. NML Cyg	−1.93	−3.04	−5.17	−5.77	3.84	13	...	...
63. R Dra	+2.03	+1.63	+0.90	+0.44	1.79	2.9	M5–M7	M
64. α Her	−3.69	−3.48	−3.80	−4.06	0.37	0.09	M5 II	SRc
65. g Her	−2.18	−2.07	−2.33	−2.66	0.48	0.07	M6 III	SRb
66. U Her	−0.78	−1.11	−1.67	−2.59	1.71	2.6	M7–M8	M

NOTE.—46, 47, 62, 96, 97 from CIT catalog; 68 ≡ CIT 7; 69 ≡ CIT 9; 84 ≡ CIT 8; 61 observed at 3.5 μ minimum.

TABLE 1—*Continued*

Star	3.5 μ	4.9 μ	8.4 μ	11 μ	[3.5] −[11]	dM/dt $\times 10^{-6}$ $M_\odot$ yr^{-1}	Spectral Type	Variable Type
M Giant Variables								
67. X Her	−1.65	−1.40	...	−3.18	1.53	0.5	M6	SRb
68. RU Her	−0.15	−0.36	−1.04	−1.99	1.84	4	M7	M
69. MW Her	+0.36	−0.03	−1.18	−2.35	2.71	5	...	M
70. OP Her	+0.03	+0.24	−0.38	−0.74	0.77	0.23	M6	Ib
71. R Hya	−3.16	−3.23	−3.69	−4.62	1.46	0.7	M7	M
72. W Hya	−3.67	−4.29	−4.60	−5.45	1.78	2.0	M7–M9	M
73. R Leo	−3.25	−3.59	−4.02	−4.93	1.78	2.0	M7–M9	M
74. VY Leo	−0.96	...	−0.90	−1.24	0.28	0.06	M5 III	Ib
75. R LMi	−1.15	−0.96	−2.15	−2.83	1.68	3	M7–M8	M
76. RS Lib	−0.25	−0.31	−0.85	−1.69	1.44	1.1	M7–M8	M
77. R Lyr	−2.32	−2.11	...	−2.80	0.48	0.09	M5 III	SRb
78. XY Lyr	−0.60	−0.62	...	−1.26	0.66	0.4	M4	Ib
79. Y Lyn	−0.66	−0.40	...	−1.40	0.74	0.23	M5 Ib–II	SRc
80. X Oph	−1.45	−1.49	...	−2.76	1.31	0.9	M5–M7	M
81. U Ori	−1.20	−0.93	−1.80	−2.82	1.62	1.2	M8	M
82. TW Peg	−0.85	...	...	−2.26	1.41	0.5	M7	SR
83. τ^4 Ser	−1.25	−1.11	−1.48	−2.08	0.83	0.13	M6	Ib
84. WX Ser	+1.60	+1.05	−0.33	−1.28	2.88	8	M8	M
85. Z UMa	−0.03	+0.31	...	−0.90	0.87	0.28	M5–6	SRb
86. RY UMa	+1.98	+2.40	+1.39	+0.19	1.79	0.4	M2–M3 III	SRa
87. U UMi	+0.58	+0.40	−0.09	−0.72	1.30	1.4	M6	M
Carbon Stars								
88. S Cep	−1.64	−2.02	...	−2.91	1.27	...	C7,4	M
89. Y CVn	−1.36	−1.11	−1.97	−1.95	0.59	...	C5,4	SRb
90. U Cyg	+0.65	+0.24	−0.57	−1.40	2.05	...	C8,2	M
91. V460 Cyg	−0.27	...	...	−1.04	0.77	...	C6,5	M
92. V Hya	−1.80	−2.29	−3.52	−4.12	2.32	...	C6,3	M
93. T Lyr	−0.43	...	...	−1.55	1.12	...	C5,3	Ib
94. V Oph	+1.13	+0.87	+0.22	+0.06	1.07	...	C6,3	M
95. TX Psc	−0.87	...	...	−1.37	0.50	...	C6,2	Ib
96. CIT 6	−2.33	−4.59	−4.78	−5.44	3.11	...	...	...
97. +10°216	−2.83	...	−6.60	−7.34	4.41	...	...	...
H-Deficient stars								
98. R CrB	+2.60	+1.67	+0.18	−0.06	2.66	...	Gp	RCB
99. β Lyr	+2.82	+2.45	+2.24	+1.96	0.86	...	B9 II	E
100. υ Sgr	+1.19	...	...	−1.65	2.84	...	Ap	E
101. BD+10°2179	...	>+6.0	...	...	...	...	Bp	...
Late Stars with Early Companions								
102. R Aqr	−2.31	...	...	−4.43	2.12	...	M7	...
103. W Cep	+1.82	+1.03	−0.37	−1.70	3.52	...	K0 Ia	SRc
104. VV Cep	−0.48	...	...	−0.69	0.21	...	M2 Ia	E
105. o Cet	−3.49	...	...	−5.45	1.96	...	M6	M
106. T CrB	+4.54	+4.24	+3.54	>3.5	<1.0	...	M2	N
107. RW Hya	+4.25	+4.08	...	+2.87	1.38	...	M2	N
108. XX Oph	+2.47	+2.43	+1.54	+1.27	1.20	...	Be	?
109. α Sco	−4.19	−3.99	−4.36	−4.82	0.63	...	M1 Iab	SRc
110. FR Sct	+2.47	+1.70	+1.13	+0.70	1.77	...	M2.5 Iab	Ib

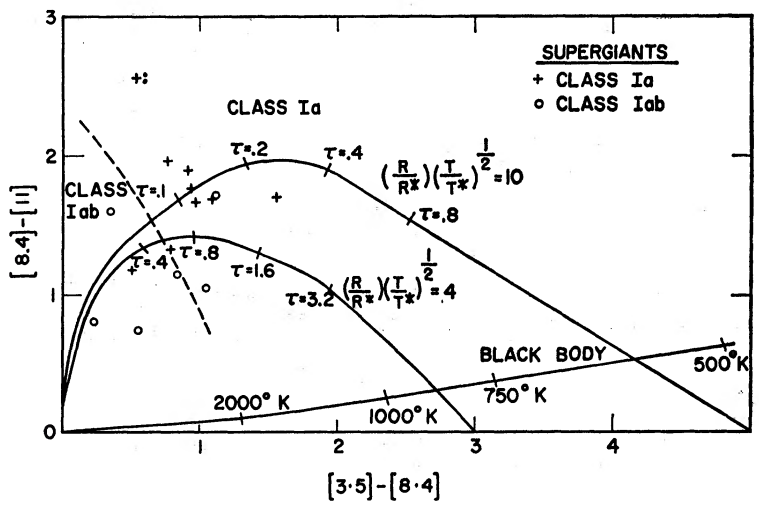

FIG. 1.—Color-color diagram for late-type supergiants. *Solid curves*, calculated as described in the text. *Dashed line*, apparent separation of different luminosity classes in the diagram.

that the concept of a shell separated from a star is probably correct. Further, we can associate the optical depth of the envelope of a star with the theoretical optical depths adopted in drawing the curves. Thus, e.g., BC Cygni shell has an optical depth ~0.15 at 11 μ. Since the shell opacity at 3.5 μ is finite, the theoretical curves will be in error for envelopes with large optical depths.

Unfortunately, it is difficult to derive the shell temperature from this diagram. Also, the suggestion by Woolf and Ney that the shell temperature was ~300° K for R Aqr was derived under the assumption of a very large optical depth for that shell and for that reason is probably incorrect. It is remarkable that in all of the observations of M stars given here, none seem to fall below the blackbody line, although the theory permits this to happen for hot shells. If the interception with the blackbody lines gives the shell temperatures, then we shall find shell-dust temperatures of ~600° K for supergiants and 800° K for giants. On the other hand, for densities that will be derived, the partial pressure of silicate gas and grains should be equal near 1200° K. It should be possible to determine shell temperatures from the ratio of fluxes near 11 and 20 μ, but current observations and calibrations available to us do not yet seem adequate. We shall adopt a temperature for the dust of 900° K in all calculations. Thus, e.g., for BC Cygni, the stellar effective temperature is 3000° K, so the shell radius is 18 stellar radii, or approximately 2×10^{15} cm. Note that the supergiants of different luminosity classes fall in different regions of Figure 1.

Similar plots are also possible for Mira variables and other lower-luminosity giant stars. Here it is found that to match the observations the opacity ratio is best set at 5:1:0, a difference perhaps explained by a change in the ratio of SiO_4 bonded matter to SiO_3 bonded matter under different condensation conditions. It is seen that a large range of shell sizes must be present. The typical lower-luminosity star with a shell has an effective temperature of 2700° K, and the shell size is about 4 stellar radii, or about 1.6×10^{14} cm for a typical Mira variable.

Figure 2 shows giant stars, with separate symbols to mark different types of object. It is seen that the type of variable defines the region of the diagram in which it falls. The typical 11-μ optical depths are 1 for Mira variables and SRa variables which are like Miras in all but amplitude. SRb and some low-luminosity SRc variables have optical depths of ~0.25, while Ib stars have optical depths of ~0.15. Stars classified as nonvariable or mildly variable have shells with very small optical depths. Three very red

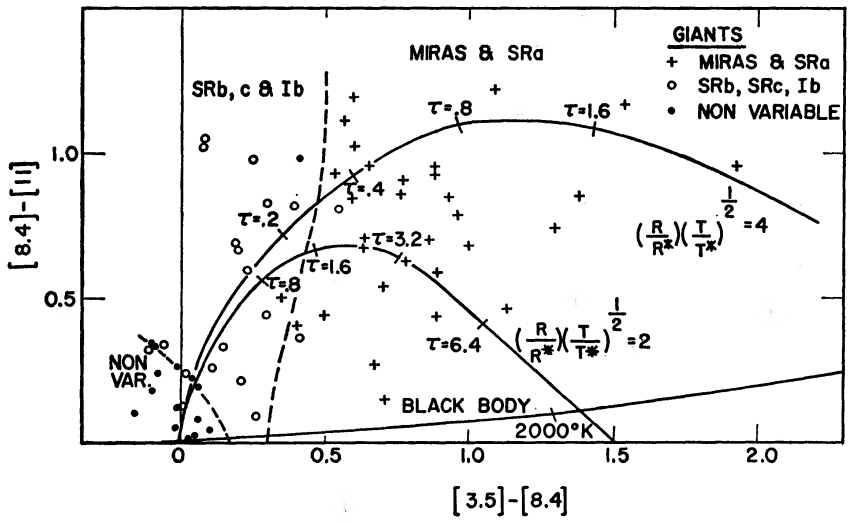

FIG. 2.—Color-color diagram for late-type giant stars. *Solid curves*, calculated as described in the text; *dashed lines*, apparent separation of classes of variable in the diagram.

objects from the CIT 2-μ survey (Ulrich *et al.* 1966) have typical optical depths of $\sim$2. The earliest-type Miras have relatively smaller shells of greater optical depth than the later type.

V. MASS FLOW VELOCITIES OF DUST AND GAS

Consider a shell of dust and gas around a star. The dust will acquire a terminal velocity V_T with respect to the gas. For supersonic flow,

$$V_T = \left(\frac{LQ_p}{8\pi X^2 \rho_g c}\right)^{1/2}, \tag{2}$$

where L is the luminosity of the star, Q_p is the effective cross-section for radiation pressure for a grain in units of its geometric cross-section, X is the distance from the center of the star, ρ_g is the gas density, and c is the velocity of light.

The gas molecules accelerated by the grains impart their momentum to the rest of the gas. We assume that pressure effects, gas heating, and gravitational forces absorb some energy, so we determine the velocity of the gas from the conservation of energy:

$$V_g \leq \left[\left(\frac{1}{X_0} - \frac{1}{X}\right)\left(\frac{f_{gr}}{f}\frac{3L}{8\pi c}\frac{Q_p}{a\rho}\right)\right]^{1/2}, \tag{3}$$

where V_g is the gas velocity, X_0 is the distance from the star center to the base of the flow, f_{gr}/f is the fraction of the outflowing mass in the form of solids, ρ is the density of a grain, and a is the grain radius.

As an example, consider a Mira star for which $L = 4 \times 10^{37}$ ergs sec^{-1}, $X_0 = 10^{14}$ cm, $Q_p = 0.03$, $a = 3 \times 10^{-6}$ cm, $\rho_g = 2 \times 10^{-16}$, $\rho = 3$, and $X = \infty$ cm. Then $V_T = 9$ km sec^{-1}; and for $f_{gr}/f = 1/250$, $V_g \leq 48$ km sec^{-1}.

Observations of circumstellar line velocities in giants and supergiants have been made by Deutsch (1960). Outflow velocities varied from 25 to 8 km sec^{-1} for giants, and 21 to 5 km sec^{-1} for supergiants. Further, from observations in the spread of velocities of OH and H_2O masers around cooler stars (Schwartz and Barrett 1970), outflow velocities for envelopes of these stars are similar to giants and supergiants. Thus the calculated example is compatible with the velocity observations. We can expect that for grain formation, the radiation density must reach some critical value, thus L/X_0^2 should be approximately constant from star to star. Then $L/X_0 \propto L^{1/2}$, and $V_g \propto L^{1/4}$. The small range in the observed gas velocities is a consequence of the modest range in bolometric luminosities of these cool late-type stars.

VI. RATES OF MASS LOSS

The dust density in the envelope d and the optical depth of silicates τ can be related to the envelope dimensions. At a constant gas velocity, the density would fall off as X^{-2}. If the dust density does the same, then the mean optical depth of the emission region can be shown to be equal to that from a region of density equal to the shell's inner density, and of thickness somewhat less than the shell's inner radius.

The optical depth of $MgSiO_3$ at 11 μ is 2.5×10^3 g^{-1} cm^2 (Gaustad 1963). Other silicates have opacities that are very similar. Thus, if we allow for the average path length through the shell of 4 times the shell thickness,

$$d = \frac{\tau}{10^4 X_0} \text{ g cm}^{-3}. \tag{4}$$

Now if the gas velocity is large compared with V_T, the gas density will be $250d$. If the gas density is low, this will not hold, and its density will be higher by some factor F_V. The rate of mass loss from the star, if a gas velocity of 10 km sec^{-1} is assumed, is

$$\frac{dM}{dT} = 4\pi R^2 \rho_g V_g , \quad \text{or} \quad \frac{dM}{dT} = F_V 5.10^{-21} X_0 \tau M_\odot \text{ year}^{-1} . \tag{5}$$

The optical depth can be obtained from the photometry for thin envelopes,

$$\tau = \left(\frac{T^*}{900}\right)\left(\frac{R^*}{R_{\text{envelope}}}\right)^2 \{\text{antilog}_{10}\, 0.4([3.5] - [11]) - 1\} . \tag{6}$$

Thus

$$\frac{dM}{dT} = 5.10^{-21} F_V \left(\frac{T^*}{900}\right)\left(\frac{R^*}{R_{\text{envelope}}}\right) \{\text{antilog}_{10}\, 0.4([3.5] - [11]) - 1\} .$$

For optically thick envelopes, the [3.5] − [8.4] colors can be used instead.

The adopted values of F_V are obtained with the use of equations (1) and (2), and with some assistance from observed values of outflowing gas velocities. We adopt a value for F_V of 1.5 for Mira stars, of 4 for BC Cygni, and of 2.5 for α Ori and α Her.

The following average rates of mass loss for these stars are obtained by using typical radii and temperatures of supergiants from Lee (1970), and for Mira stars by Smak (1966):

Mira Stars:	$2 \times 10^{-6}\ M_\odot$ year^{-1} ;
α Her:	$9 \times 10^{-8}\ M_\odot$ year^{-1} ;
α Ori:	$7 \times 10^{-7}\ M_\odot$ year^{-1} ;
BC Cygni:	$7 \times 10^{-6}\ M_\odot$ year^{-1} .

The ratio of the rates for α Her and α Ori is consistent with the observation reported by Weymann, but the rates given here are smaller by a factor of 6. The rates calculated here would be larger if not all of the silicon were in dust.

The rates of mass loss for the Miras seem to vary among the different groups, and there is some indication that the rates are higher among the longer-period cooler group which is more concentrated to the galactic disk. Of the objects given in Table 1, there are four cool objects specially selected as being very red in the CIT survey. The mean rate of mass loss for these stars is $7 \times 10^{-6}\ M_\odot$ year^{-1}, whereas for other Miras the average is 1.7×10^{-6}. SRa variables average 1.5×10^{-6}, SRb and SRc (class Ib–II) stars average 0.3×10^{-6}, while Ib's average 0.2×10^{-6}. For the supergiants, the average rate is 7×10^{-6}, with a steep decrease of the rate with decreasing luminosity. The rates for individual stars seem to have an appreciable spread even when otherwise similar stars are compared. The phenomenon of circumstellar emission in the giants first becomes noticeable at class M3 III, and the infrared excess seems to double for each later spectral class to M6 III. The rates of mass loss probably more than double for each change of spectral class. Earlier M-type variable stars seem to have greater rates of mass loss than nonvariable stars. Supergiants seem to develop observable emission at progressively earlier spectral types as one considers progressively higher luminosity classes, with large emission from the most luminous late G-type stars.

VII. GALACTIC CONSEQUENCES

Oort and van Tulder (1942) give a density distribution of 0.1 long-period variables per 10^6 pc^3, and a scale height of 1500 pc. There are then 3×10^{-4} stars pc^{-2} projected onto the galactic plane, and the mass returned to the Galaxy from the Miras is about $6 \times 10^{-10}\ M_\odot$ year^{-1} pc^{-2}. Further, if we assume that the other cool stars in the halo and disk augment this flow by ~20 percent, we find a total rate of mass loss from the halo and disk stars of $7 \times 10^{-10}\ M_\odot$ year^{-1} pc^{-1}.

From theoretical stellar death rates and observed stellar densities Deutsch (1968) has estimated a total rate of mass return for the region of the Galaxy near the Sun as $4 \times 10^{-10}\ M_\odot$ pc^{-2}. This rate is less than that calculated from the Mira stars alone.

This result is a pleasant change from previous calculations which had always seemed to show insufficient mass leaving stars (Woolf 1966). Presumably the two estimates may now converge. Further, with these results the high abundance of silicates in interstellar space can be understood as a consequence of its injection by cool stars.

In contrast to these results, the mass return from M supergiants does not seem to add up to any large fraction of the rate of mass loss expected from their deaths. The detailed matching of late-type stars to the particular mass range of their progenitors may help explain this discrepancy. However, some of the mass of the more massive stars may well be lost in other evolutionary phases.

VIII. CONCLUSIONS

Observations of cool stars have been interpreted to give rates of mass loss. These rates are adequate to explain the abundance of silicate dust in interstellar space, and seem adequate to resupply the interstellar matter used up in star formation.

Color-color diagrams show that supergiants have envelopes with optical depths and relative radii with respect to their stellar radii that are luminosity class dependent. Lower luminosity class stars similarly fall into groups that are characterized by their type of variability or lack of it.

This study was greatly influenced by an unpublished paper by Gilman (1966). We are indebted to Drs. Stein and Gillett for the use of their equipment, advance communication of their results, and discussions. D. W. Strecker assisted with many of the observations at the O'Brien Observatory. We would like to acknowledge stimulating discussions and communication of unpublished results from Drs. E. Becklin, M. Dyck, G. Herbig, G. Neugebauer, E. Ney, P. Solomon, and R. Weymann.

This research has been supported by grants NGL-24-005-063 and NGL-24-005-008 from NASA and by the Graduate School of the University of Minnesota. R. D. G. is an NSF trainee.

REFERENCES

Arrhenius, G., and Alfvén, H. 1971, to be published.
Deutsch, A. J. 1960, in *Stars and Stellar Systems*, Vol. **6**, ed. J. L. Greenstein (Chicago: University of Chicago Press), p. 543.
———. 1968, in *Mass Loss from Stars*, ed. M. Hack (Dordrecht: Reidel Publishing Co.), Vol. 1.
Dyck, H. M., Gillett, F. C , Forrest, W., Stein, W. A., Gehrz, R. D , and Woolf, N. J. 1971, *Ap. J.*, **165**, 57.
Gaustad, J. E. 1963, *Ap. J.*, **138**, 1050.
Gehrz, R. D., Ney, E. P., and Strecker, D. 1970, *Ap. J. (Letters)*, **161**, L219.
Gehrz, R. D., and Woolf, N. J. 1970, *Ap. J. (Letters)*, **161**, L213.
Gillett, F. C., Hyland, A. R., and Stein, W. A. 1970, *Ap J. (Letters)*, **162**, L21.
Gillett, F. C., Merrill, K. M., and Stein, W. A. 1971, *Ap. J.*, **164**, 83.
Gillett, F. C., and Stein, W. A. 1971, *Ap. J. (Letters)* (in press).
Gilman, R. C. 1966, unpublished manuscript.
———. 1969, *Ap. J. (Letters)*, **155**, L185.
Hackwell, J. H., Gehrz, R. D., and Woolf, N. J. 1970, *Nature*, **227**, 822.
Hardie, R. H. 1962, in *Stars and Stellar Systems*, Vol. **2**, ed. W. A. Hiltner (Chicago: University of Chicago Press), p. 191.
Johnson, R. L. 1965, *Comm. Lunar and Planet. Lab*, No. 53.
Lee, T. A. 1970, *Ap. J.*, **162**, 217.
Ney, E. P. 1969, private communication.
Ney, E. P., and Allen, D. A. 1969, *Ap. J (Letters)*, **155**, L193
Oort, H. D., and van Tulder, J. J. M. 1942, *B.A.N.*, **9**, 327.
Saiedy, F. 1960, *M.N.R.A.S.*, **121**, 483.
Schwartz, P. R., and Barrett, A. H. 1970, *Ap. J. (Letters)*, **159**, L123.
Smak, J. F. 1966, *Ann. Rev. Astr. and Ap.*, **4**, 19.
Stein, R. F. 1966, *Stellar Evolution*, Vol. **3**, ed. R. F. Stein and A. G. W. Cameron (New York: Plenum Press).
Stein, W. A., and Gillett, F. C. 1969, *Ap. J. (Letters)*, **155**, L197.

Ulrich, B. T., Neugebauer, G., McCammon, D., Leighton, R. B., Hughes, E. E., and Becklin, E. 1966, *Ap. J.*, **146**, 288.
Weymann, R. J. 1962, *Ap. J.*, **136**, 844.
Wickramasinghe, N. C., Donn, B. D., and Stecher, T. P. 1966, *Ap. J.*, **146**, 590.
Wilson, O. C. 1960, in *Stars and Stellar Systems*, Vol. **6**, ed. J. L. Greenstein (Chicago: University of Chicago Press), p. 436.
Woolf, N. J. 1966, *Ap. J.*, **145**, 649.
Woolf, N. J., and Ney, E. P. 1969, *Ap. J.* (*Letters*), **155**, L181.
Woolf, N. J , Stein, W. A., and Strittmatter, P. 1970, *Astr and Ap.*, **9**, 252.